# 5

# Organic Humidity Sensor for Healthcare Applications

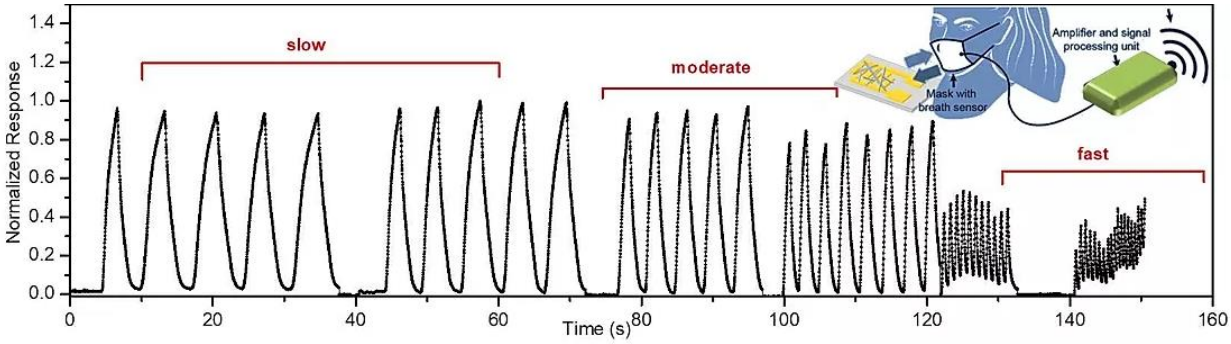


## 5.1 Introduction

Humidity sensors play a vital role today in providing information about optimum environmental conditions for human comfort in addition to their use in medical, ceramics, chemical, and food industries [Farahani et al., 2014]. The multifunctional application of humidity sensors in breath rate monitoring, touch-free skin examination, non-contact switch, and spatial localization monitoring has created a surge in recent past. Mostly, humidity sensors response are either capacitive, resistive, or optical at variable humidity conditions [Chen et al., 2005b].

### 5.1.1 Objectives of Work

The objectives of this work are as follows:

1. To study a novel organic system, N-F containing crystals of Selectfluor™ (F-TEDA) as an organic material for the fabrication of the humidity sensor.
2. To optimize the fabrication process and conditions for selective, sensitive, fast and stable humidity sensor.
3. To test the humidity sensor for monitoring the breath rate and skin moisture response for continuous non-invasive physiological monitoring.

## 5.2 Experimental

### 5.2.1 Device fabrication

Cleaned glass substrates were used for the fabrication of gold interdigitated electrodes (IDE). Photolithography was used for the fabrication of µm-sized interdigitated electrodes. For the fabrication of humidity sensor, a 2µL drop of 100 mM fluorotriethylenediammonium bis(tetrafluoroborate), F-TEDA (Sigma Aldrich, CAS No. 140681-55-6) in acetonitrile (Sigma Aldrich, 99.8%) was drop-casted on the IDE, followed by drying under room temperature until crystallization. Copper wire contacts were made using silver paste for electrochemical measurements.

### 5.2.2 Characterization

FESEM imaging and EDX mapping was done using Nova NanoSEM 600 (FEI Co., The Netherlands). FTIR spectra of F-TEDA in the dry and wet state were recorded on Bruker Vertex 70 V+PMA50 spectrometer. Electrochemical workstation (CH instruments, 660E) was used to carry out Linear Sweep Voltammetry (LSV), Cyclic Voltammetry, I-t measurements and Electrochemical Impedance Analysis (EIS).

### 5.2.3 Humidity Sensing setup

For carrying out the measurements under different RH conditions, a constant humidity was generated in a custom-made environmental chamber using commercial ultrasonic mist humidifier. The environmental chamber was equipped with a reference commercially available humidity sensor (Testo 410-2) to read the humidity values inside the chamber for calibration. Nitrogen gas was used to evacuate the chamber for lower RH values (Figure 5.1).

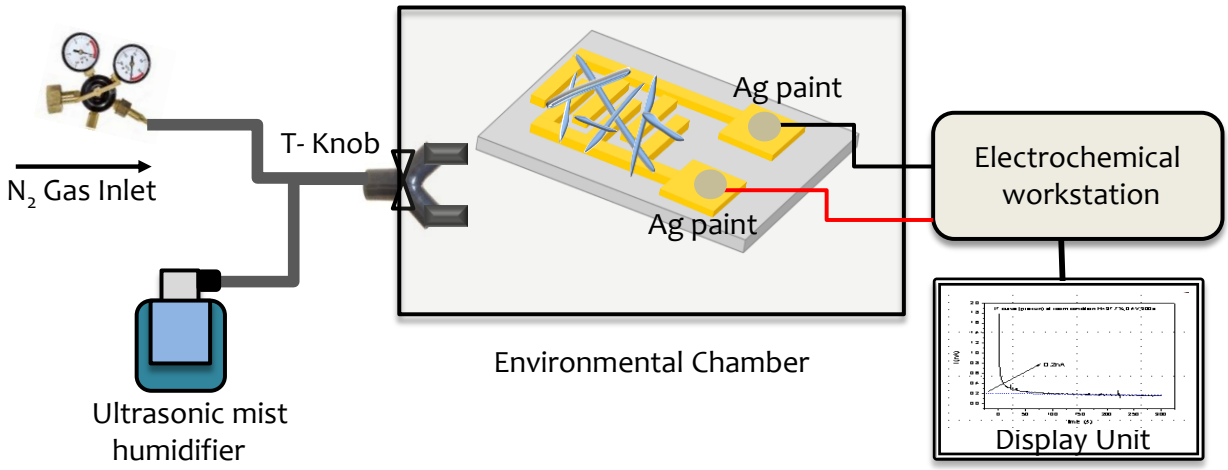


**Figure 5.1:** Schematic diagram showing the setup used for the characterization of a humidity sensor.

### 5.2.4 Humidity Sensing Characteristics

F-TEDA based humidity sensor was loaded in the chamber for the simultaneous electrical response of the device at different humidity conditions. To examine the specificity of the sensor, different **VOCs** were vaporized by bubbling of nitrogen gas, which was allowed to enter the device chamber (in the form of a pulse of 1 minute) maintained at 10% RH. The stability of the sensor was evaluated for prolonged durations at 95% humidity. Response time was measured by blowing human breath and recovery time measurements by purging $N_2$ gas quickly. A volunteer was chosen and instructed to 'inhale and exhale' at different breathing frequency for breath monitoring tests. Further, the breathing rate was calculated by taking the mean of five inhale and exhale cycles. The device was also prepared on a flexible PET substrate and the humidity response was recorded at a bending angle of 57°.

## 5.3 Result and Discussion

### 5.3.1 Optimization of Sensor

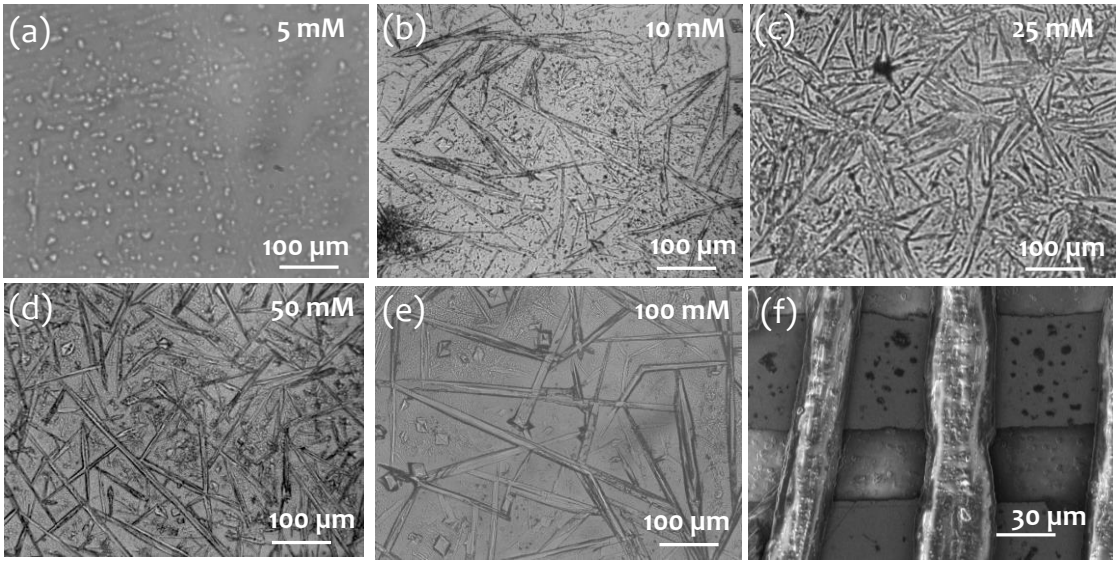


**Figure 5.2:** Optical photographs of crystals of F-TEDA prepared using different concentrations of solution (a) 5 mM, (b) 10 mM, (c) 25 mM, (d) 50 mM and (e) 100 mM. (f) SEM image of F-TEDA crystals (100mM) on IDE.

Different solutions of F-TEDA (5, 10, 25, 50 and 100 mM) in acetonitrile were drop-coated on the pre-cleaned glass slides, and crystals were examined under an optical microscope as shown in Figure 5.2a-e. At low concentration of 5 mM (Figure 5.2a), tiny seeds are observed indicating the nucleation of crystals. At higher concentration (10 mM), the crystals growth occur longitudinally and thin, needle-shaped crystals of ~150-200 µm length are observed sparsely distributed over the surface (Figure 5.2b). Interestingly, crystals form a densely interconnected network at 25 mM (Figure 5.2c). With further increase in concentration (50 mM, Figure 5.2d), F-TEDA crystallizes as well-defined needle-shaped crystals that grow thicker ~20 µm and longer (~1 mm) at 100 mM interconnecting easily due to the high aspect ratio of ~1000 (Figure 5.2e and 5.4f). No solutions could be prepared with concentrations above 100 mM due to the solubility limit of F-TEDA in acetonitrile.

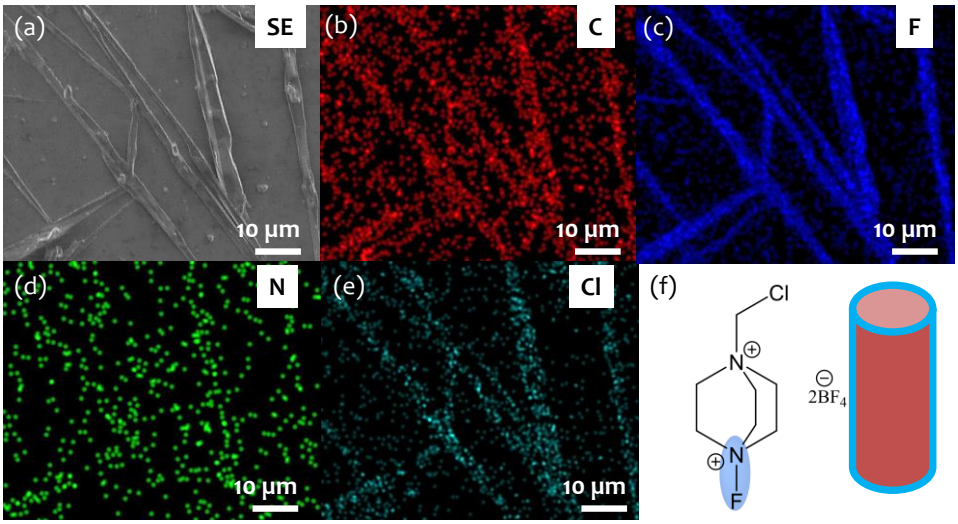


**Figure 5.3:** (a) Secondary electron image and the corresponding elemental maps of (b) C, (c) F, (d) N and (e) Cl and (f) molecular structure of F-TEDA.

Owing to the length of crystals and limited solubility in water and other polar solvents (0.1-0.5 g/L), F-TEDA crystals are directly used as an active material for the fabrication of humidity sensor. For the purpose, different devices were fabricated by drop-casting F-TEDA solutions of 25, 50, and 100 mM concentration directly on Au IDE followed by slow evaporation leading to crystallization. The elemental mapping of the F-TEDA crystal (secondary image in Figure 5.3a)

are shown in Figure 5.3 b-e. It can be seen that the elements C, F, N and Cl are distributed in the crystal. As expected, the signal of fluorine is much more intense at the surface as compared to other elements due to the presence of $BF_4^-$ shell around the organic part of the F-TEDA molecule (Figure 5.3c). Thus, F-TEDA molecule shown in Figure 5.3f can be represented with a 1D model crystal structure with a core consisting of the organic unit and the surface covered with fluorine atoms that are sensitive to water molecules.

**Table 5.1:** Details of the humidity sensing devices fabricated in this study.

| Device* | Conc. (mM) | Type | Sensitivity ($\times 10^6$) |
|---|---|---|---|
| **1** | 25 | IDE-1 | 0.99±0.04 |
| **2** | 50 | IDE-1 | 2.04±0.04 |
| **3** | 100 | IDE-1 | 3.23±0.03 |
| **4** | 100 | IDE-1 | 2.80±0.02 |
| **5** | 100 | IDE-1 | 3.01±0.06 |
| **6** | 100 | IDE-2 | 1.15±0.05 |
| **7** | 100 | IDE-2 | 1.06±0.04 |
| **8** | 100 | IDE-2 | 1.21±0.04 |

*All the devices are operated at 0.8 V.
Maximum Error in Sensitivity is less than 5%

All the humidity sensing devices fabricated in this study with different parameters such as concentration and electrode geometry are summarized in Table 5.1. The performance of the F-TEDA crystals towards humidity was analyzed over different geometry of interdigitated electrodes with electrode geometrical parameters tabulated in Table 5.2.

**Table 5.2:** Specifications of IDE-1 and IDE-2.

| | IDE-1 | IDE-2 |
|---|---|---|
| Area ($cm^2$) | $0.56\times10^{-3}$ | $1.44\times10^{-3}$ |
| Finger width (µm) | 20 | 20 |
| Finger gap (µm) | 20 | 20 |
| Number of fingers | 6 | 16 |
| Finger length (µm) | 410 | 410 |
| Sensitivity | $3.23\times10^6$ | $1.21\times10^6$ |

### 5.3.2 Characteristics of Humidity Sensor

Figure 5.4a shows the optical image of the interdigitated Au electrode with 6 fingers of width ~20 µm separated by ~20 µm (IDE-1) with thick F-TEDA crystals grown longitudinally and positioned perpendicularly across the interdigitated fingers, thus, ensuring physical contact required for electrical conduction between the evenly spaced gold electrodes. The humidity response was studied in a custom-designed set up shown in Figure 5.1.

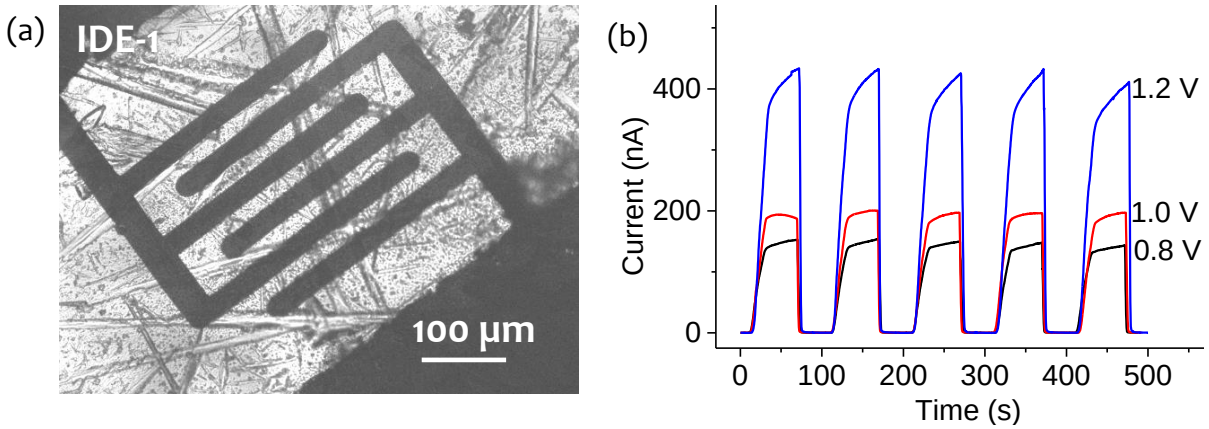


**Figure 5.4**: (a) Optical photograph and (b) Current response as RH is switched between 10% and 95% at different applied voltages (0.8, 1.0 and 1.2 V).

The device was exposed to different percentages of relative humidity that was measured using a commercial humidity meter. Nitrogen gas with 95% RH was passed through the humidity chamber for electrical characterization in the closed chamber. The device was subjected to RH cycling between 10% and 95% at applied voltages of 0.8, 1.0 and 1.2 V respectively (Figure 5.4b). At 0.8 and 1.0 V, the current response was observed to be nearly constant over repeated cycles as the RH value is switched between 10% and 95%. However, despite higher current response, the device took much longer to achieve a steady-state at 1.2 V, indicating higher response time. Hence, 0.8 V was chosen as an optimum voltage for the operation of the F-TEDA-based humidity sensor.

### 5.3.3: Sensitivity of Humidiy Sensor

The sensitivity values at different RH% were calculated in reference to 10% RH using the equation given in literature considering only resistive nature of the device [Ali et al., 2016; Kuang et al., 2007; Mogera et al., 2014]:

$$S_x = \left(\frac{I_{RHx\%} - I_{RH10\%}}{I_{RH10\%}}\right) \times 100 \qquad \ldots.(1)$$

where $S_x$ is the sensitivity at relative humidity values of $x$, $I_{RHx\%}$ is the current value at relative humidity value of $x$% and $I_{RH10\%}$ is the current value at relative humidity value of 10%. The sensitivity of devices 1, 2 and 3 at all humidity values is shown in Figure 5.5a.

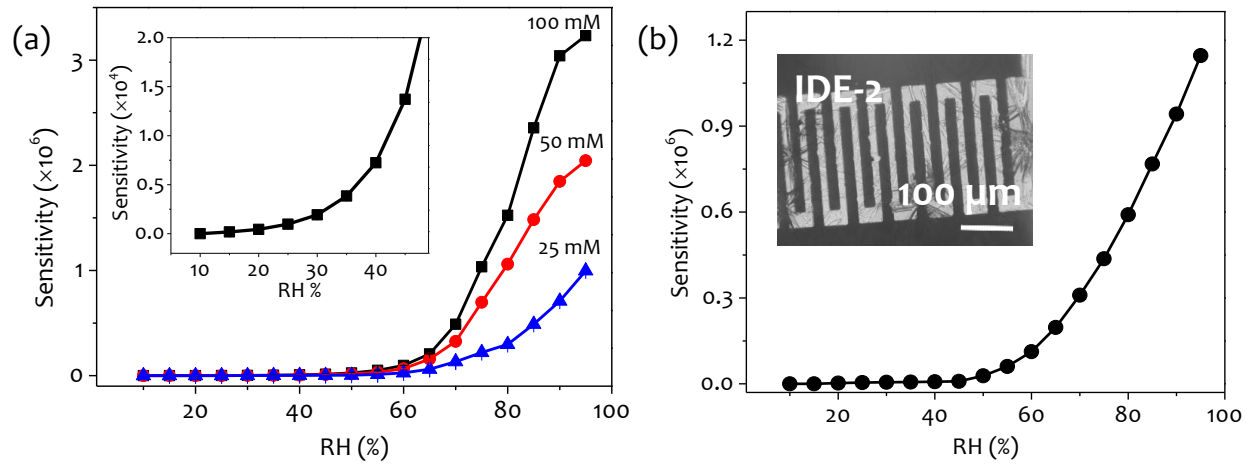


**Figure 5.5** (a) Sensitivity of device 1, 2 and 3 at different humidity values fabricated using solutions of 25, 50 and 100 mM concentration on IDE-1. Inset shows the sensitivity of the *device-3* at lower humidity values (b) Sensitivity of *device-6* at different humidity values fabricated on IDE-2. Inset shows the optical photograph of

the device. (Note: The error bars in a and b have been plotted with respect to mean of values over 50 s of continuous and stable data collection).

All the fabricated devices show an exponential increase in sensitivity with the corresponding humidity change. In low RH%, sensitivity value is ~4 order of magnitude which is reasonable (inset, Figure 5.5a). However, it is interesting to observe a steep rise in sensitivity beyond 50% RH (~$10^5$ at 70% and ~$10^6$ at 95%). The device-3, 4 and 5 tabulated in Table 5.1 prepared using 100 mM solution under similar conditions exhibits ~3 times higher sensitivity ($3.01\times10^6\pm0.05$) as compared to device-1 on exposure to humidity. It is probably due to lesser contact resistance and longer percolation channel for the water molecules in thick and long crystals resulting in higher current across the device. The overall sensitivity is of the order of 6 and to the best of our knowledge, such high sensitivity values have not been reported in the literature (Table 5.1). Device-6 was fabricated on a different electrode geometry (IDE-2) with 16 fingers of ~20 µm widths and electrode spacing of ~20 µm to study the influence of electrode area and geometry on the performance of the humidity sensor (inset, Figure 5.5b, and Table 5.1). The sensitivity of device-6 with respect to different RH% is shown in Figure 5.5b. Clearly, IDE-2 fabricated with 100 mM F-TEDA shows a similar trend in the humidity response as that of IDE-1 however the sensitivity is ~2.8 times lower than device-1 probably due to higher contact resistance between the physically placed crystals and electrodes with an increase in the number of contact fingers in IDE-2 geometry. Thus a smaller device with lesser fingers and spacing is ideal for the better performing device.

Several other devices were fabricated to test the reproducibility as shown in Figure 5.6. As tested over 3 devices number 6, 7 and 8, the sensitivity of device (IDE-2) is nearly constant with a relative difference of <5%. It is because the density of crystals is dependent on the concentration of solution drop-casted on IDE and the length of crystals across the gap electrode results in the reproducible and repeatable devices.

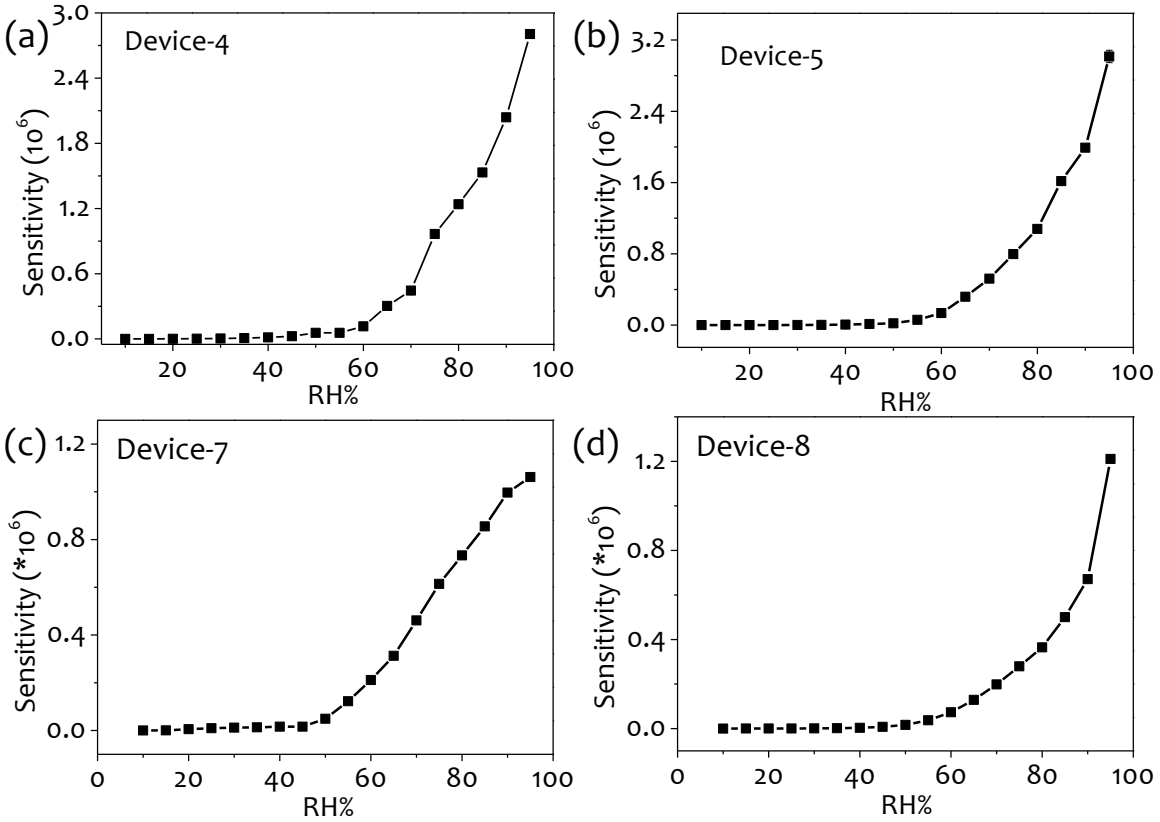


**Figure 5.6:** Sensitivity of (a) device-4, (b) device-5, (c) device-7 and (d) device-8 at different relative humidity values.

### 5.3.4 Stability of Humidity Sensor

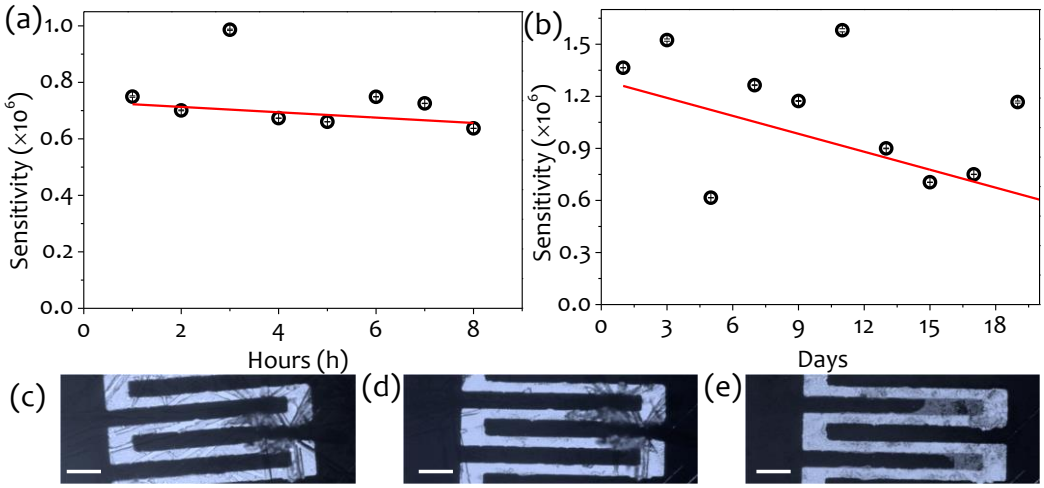


**Figure 5.7**: Variations in the sensitivity of the device at 95% RH when monitored (a) for continuously 8 hours (b) over different days. Optical photograph of crystals of F-TEDA drop-casted on Au-IDE (c) before measurement (d) 8 hour of continuous monitoring and (e) after 20 days monitoring at 95% RH (Scale bar in c- e is 100 µm).

The operational stability under extreme conditions decides the usage and lifetime of the sensor. In case of an ionic crystal based system such as F-TEDA, it may be speculated that the water vapor in humidified air might condense on the surface of the sensor and destroy the device. To quality the sensor for practical applications it is important to establish the stability and reliability by estimating the lifetime of the device. Thus, the performance of *device-6* was monitored at 0.8 V for 8 hours under continuous exposure of 95% RH as an extreme yet accelerated condition (Figure 5.7a). The device sensitivity is lowered by ~14% only even on exposure to such extreme humidity conditions. The optical photograph of a portion of the device with crystals on IDE, before and after humidity exposure for 8 hours is shown in Figure 5.7c and d respectively. It may be noted that most of the crystals are intact expect a few appear to be hazy partially due to limited depth of focus of optical microscope. Furthermore, the current output of the same *device-6* at 0.8 V was monitored over several days at 95% RH level (Figure 5.7b). The device performance gradually decreased due to continuous exposure as expected and after 20 days, the degradation resulted in a decrease in its sensitivity to 50%. This is probably due to slow dissolution of crystals and etching of Au electrodes by reactive fluorine generated from F-TEDA under an applied voltage of 0.8 V as seen in the optical photograph in Figure 5.7e. However, for practical applicability as a sensor where the exposure time is small and in fact, a fraction of second, the crystal and electrodes remains stable and unaffected because of the solubility limit of F-TEDA in water (0.1-0.5 g/L) and thus, the device is repeatedly used even after exposure to high humidity.

### 5.3.5 Specificity of Humidity Sensor

For the application of the humidity sensor in real-life conditions, selective and specific response of the sensor toward humidity is important even in the presence of volatile organic compounds (VOCs) and mixed gases to avoid any possibility of cross-interference and false signals. Thus, the sensor was subjected to various polar (acetone, chloroform, dichloromethane, isopropyl alcohol, methanol, ethanol, dimethylformamide, tetrahydrofuran, acetonitrile, ammonium hydroxide, diethyl ether) and non-polar (xylene, toluene, cyclohexane) VOCs, and other commonly occurring atmospheric gases ($CO_2$, CO, zero air) before and after exposure to short humidity pulses and the current response was recorded. The compounds were vaporized by bubbling nitrogen gas, which was allowed to enter the device chamber (in the form of a pulse of 1 minute) maintained at conditions of 10% RH to monitor even the minutest change in the

current response of the device. Remarkably, no response was observed toward any of the tested vapors (Figure 5.8).

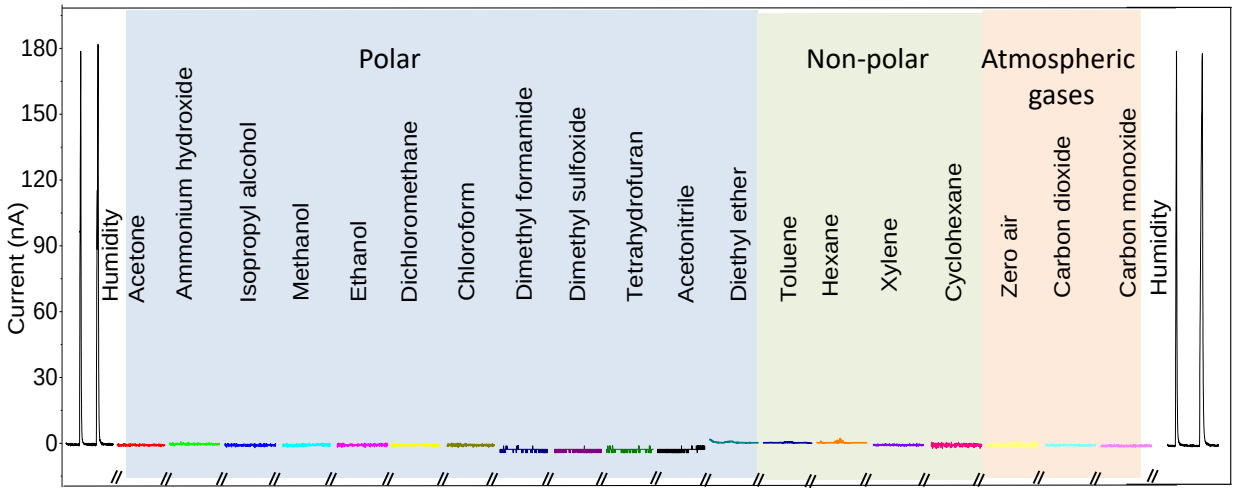


**Figure 5.8:** Current response of sensor exposed to humidity pulses before and after exposure to various volatile organic compounds (polar and non-polar) and gaseous environment.

In the crystalline state, molecule does not even respond to polar molecules and the device response remains zero. This could be attributed to the specific interaction of water molecules with polar N-F bond of the F-TEDA crystal that extends across the crystal leading to the formation of conducting water cluster network. These intruding water molecules reduce the polar interaction between the cation and the anion in the F-TEDA crystal. Molecular Dynamics simulations in literature predict a similar formation of water cluster networks with imidazolium-based ionic liquids that resembles F-TEDA structurally [Hanke et al., 2003; Jiang et al., 2007]. Furthermore, it was noticed that the device retains its sensitivity towards humidity even after exposure to extremely reactive chemical vapors as shown in Figure 5.8. This confirms the specific sensitivity of the device toward humidity, which can be explored for various practical applications of humidity sensing including moisture estimation in an environmental chamber such as glove box.

### 5.3.6 Humidity Sensing Mechanism

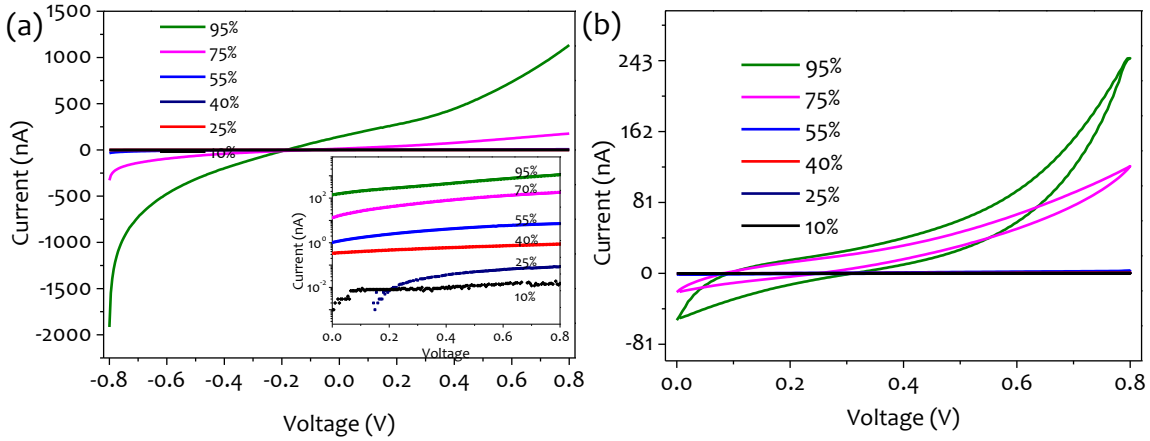


**Figure 5.9** (a) I-V characteristics (Inset: semi-log plot of I-V characteristics), (b) C-V measurements at different relative humidity (RH%) values.

I-V measurements were performed on the fabricated device at different RH% over the range of ±0.8 V to obtain mechanistic insight. At all RH conditions, the current increases with increasing voltage, indicating resistive-type behavior (Figure 5.9a). This can be clearly seen from the semi-log I-V characteristics in the inset, Figure 5.9a. At negative potentials, the device shows relatively higher current values because of the molecular rectifier-type behavior of the crystals. This asymmetric behavior is generally due to the anisotropic conduction of crystals in the

longitudinal direction. To further understand the conduction mechanism of the device, cyclic voltammetry (CV) studies were performed over the range 0–0.8 V at a scan rate of 50 mV/s at different RH% (Figure 5.9b). The current is extremely low at low RH% (<40%) indicating resistive behavior compared to the capacitive response. However, at higher humidity values (>50%), the shape of the CV loop indicates capacitive contribution along with resistive.

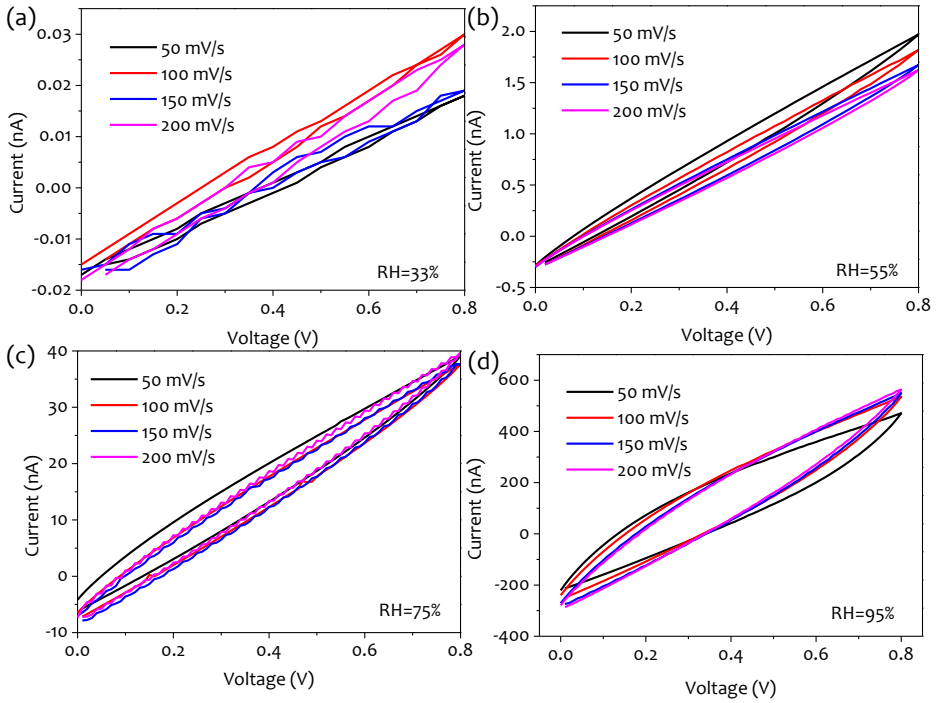


**Figure 5.10:** Cyclic voltammogram of the fabricated sensor at varying scan rates in RH conditions of (a) 35%, (b) 55%, (c) 75% and (d) 95%.

To further confirm the capacitive contribution in the humidity sensing of F-TEDA crystals, CV measurements were performed at fixed humidity values at varying scan rates of 50 -200 mV/s (Figure 5.10a-d). It was observed that at fixed humidity values (RH= 33%, 55%, 75%, and 95%), no capacitive behaviour was observed at lower humidity (33% RH and 55% RH). The specific capacitance of the device increases above 55% RH confirming the increase in capacitive contributions at higher relative humidity values.

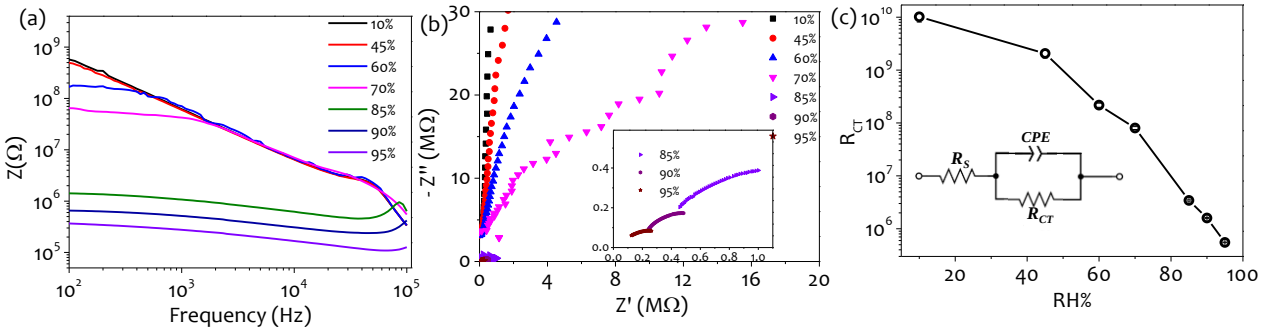


**Figure 5.11** (a) Impedance-frequency characteristics at different relative humidity (RH%) values. (b) Nyquist plot of fabricated sensor at different RH%. (c) Charge Transport Resistance ($R_{CT}$) with respect to RH%. Inset in (c) shows the corresponding equivalent circuit used for modeling. Note that error bars in (c) have been plotted with reference to the error in $R_{CT}$ for the modeled circuit.

Impedance analysis was performed under different humidity conditions over a frequency range of 0.1–100 kHz. In the plot of impedance (Z) versus frequency (Figure 5.11a), it was observed that the impedance of the device decreases with increasing values of humidity at all frequencies. In the lower frequency region of 0.1 kHz–1 kHz, four orders of decrease in the impedance can be observed with increasing RH% indicating ultrahigh sensitivity of the device (Figure 5.11a). Despite the high impedance values, the Nyquist plots show a semicircular response with decreasing diameter upon increasing the RH% (Figure 5.11b). The Nyquist plots were fitted

using an equivalent circuit comprising a resistor connected to a parallel RC circuit and the charge transfer resistance ($R_{CT}$) was estimated using the model (Figure 5.11c). Clearly, the $R_{CT}$ decreases with the corresponding increase in RH%. This type of impedance behavior has been associated with the Grotthuss conduction mechanism in literature. At lower humidity, because of the discontinuity in the Grotthuss chain, the resistance is high, while it decreases with the increase in humidity because of the formation of a continuous Grotthuss chain [Zhang et al., 2017a; Zhuang et al., 2017].

### 5.3.7 Water – F-TEDA Interaction

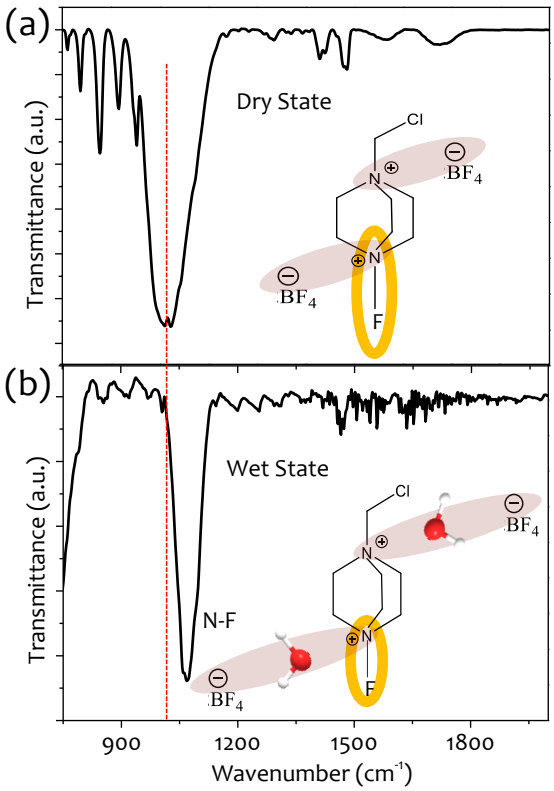


**Figure 5.12** (a,b) FTIR spectra of F-TEDA crystal in dry and wet state respectively.

The interaction of water with polar N-F bond in the molecular system is also investigated by in-situ FT-IR spectroscopy. The F-TEDA molecule under low humidity conditions (RH ~40%) exhibits a broad peak of symmetric vibration of N-F peak at 1014.4 $cm^{-1}$ (Figure 5.12a), which is significantly sharpened and shifted towards a higher wave number of 1068 $cm^{-1}$ (Figure 5.12b) under the 'wet' state with high humidity; RH= ~95%. Interestingly, this shifting in the N-F bond peak indicates the moisture sensitive nature of the compound. This could be attributed to the change in the electrostatic environment of the F-TEDA molecule upon water molecule interaction. In the presence of water molecules, the electrostatic interaction between the cation and the anion pair decreases because of solvation, resulting in an increase in the N-F bond strength [Gao et al., 2010; Jeon et al., 2008; Schenk et al., 2012]. There has been extensive research on the effect of water molecules affecting the intermolecular interaction between the cation-anion of imidazole-based ionic liquid systems and tailoring the force constant of different bonds present [Docampo-Álvarez et al., 2016; Espinosa-Marzal et al., 2014; Jurado et al., 2017]. However, a miniaturized, solid-state resistive humidity sensor is realized for the first time in this study.

### 5.3.8 Humidity Sensor as Breath Monitoring Device

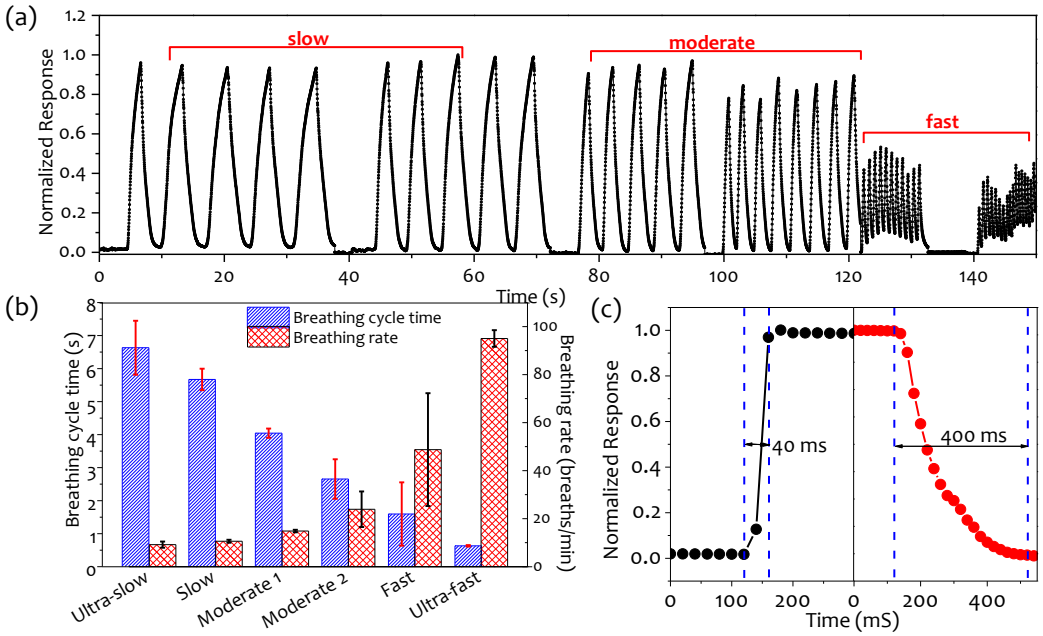


**Figure 5.13:** (a) Signals corresponding to breathing response of F-TEDA based sensor upon inhalation and exhalation at six different breathing frequencies. (b) Bar-graph representation of breathing cycle time and breathing rate calculated from human breath experiment. Note that error bars in (b) have been plotted with reference to the mean of 5 breathing cycles. (c) Normalized response curve of a typical breathing profile used for measuring the response and recovery time of the fabricated humidity sensor.

The practical application of a sensor requires a spontaneous response to external stimulus. Hence, response and recovery time along with sensitivity and stability are important parameters that determine the efficiency of a sensor especially as healthcare device for the real-time analysis of human breath rate. The sensor is mounted on a surgical mask for monitoring the breath rate as detailed in the experimental section. The breathing rate (breaths/min) was calculated by taking the average of the number of breath cycles (exhale and inhale) per unit time. The sensor responded to a wide range of breathing rates i.e. ~9.17 breath/min to ~95.03 breath/min as seen by the current response (Figure 5.13a). The double y-axis plot in Figure 5.13b depicts six different breathing rates. Higher the breathing rate, shorter is the breathing cycle time. The response and recovery time of the fabricated device was measured from a breath profile as shown in Figure 5.13c. The sensor responds to high humidity in 40 ms by blowing human breath while sensor recovery took ~400 ms as measured by quickly purging dry nitrogen gas to attain low humidity value of 10% RH (Figure 5.13c). The response and recovery time of the device is expected to be much faster than measured value and it is highly sensitive to humidity fluctuations in the high humidity range (50–95%), extreme breathing rates could be monitored spontaneously, making the sensor suitable as a breath monitoring device.

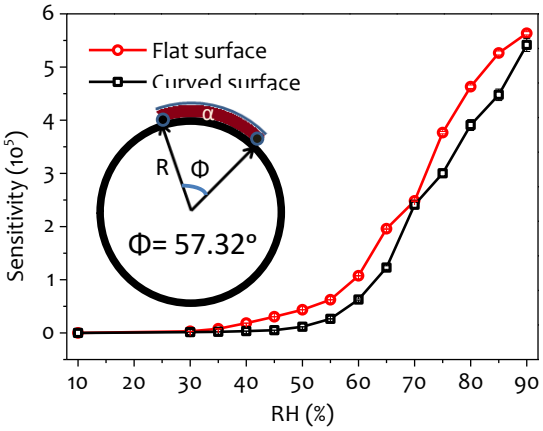


**Figure 5.14:** Flexibility of the device for wrist band application.

The flexibility of the device is one of the important aspects for wearable physiological sensors in the form of a wristband for continuous sweat monitoring. It was observed that the device showed performance analogous to rigid substrates even in the bent state, indicating its non-responsive behavior towards mechanical stress and strain (Figure 5.14).

### 5.3.9 Humidity Sensor as Touch-less Skin Moisture Sensor

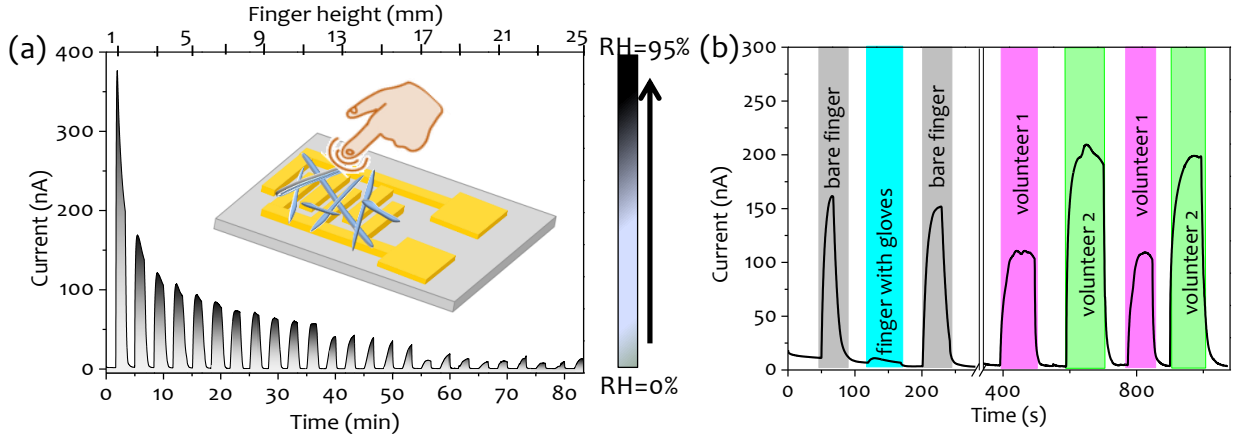


**Figure 5.15:** (a) Current response of the fabricated device at different humidity corresponding to varying finger height and (b) Skin-moisture response from human fingers of different volunteers.

The sensor can be utilized for the touch-less monitoring of moisture content of human skin. An experiment was designed to study the response of the *device-3* at different distances of a finger ranging from 1 mm–2.5 mm (Figure 5.15a). At a distance of 1 mm, the device showed very high sensitivity towards the moisture content of the human finger. As the finger was withdrawn from the sensing element, the current response decreased. A gradual decrease in the current was observed until 18 mm after which the response became almost constant (Figure 5.15a). Hence, it can be concluded that the device is extremely sensitive to the slightest changes in the moisture content of human skin. For testing the reliability and reproducibility of the sensor in real applications, the response of the sensor toward a bare finger and a finger with rubber gloves on was examined (Figure 5.15b). As expected, the sensor showed a significant increase in the current when the finger was brought close to the sensor. On the contrary, when the finger with gloves was brought in close proximity to the device, an insignificant response was observed. Furthermore, when the bare finger was again brought in proximity with the sensor, the response was repeated suggesting applications toward the real-time touch-less detection of skin moisture content. Likewise, to check the consistency of the sensor, the response of two different volunteers was recorded at a finger distance of 1mm (Figure 5.15b). Both the volunteers showed different current responses, pointing to the difference in the moisture content of individual skin type. Moreover, the response was repeated upon repeating the experiment with both the volunteers.

## 5.4 Conclusions

A solid-state humidity sensor based on organo-fluorine molecule F-TEDA crystals was successfully fabricated by a simple drop-casting technique. The sensor with a sensitivity value of ~$10^6$ (10%–95%), was found to be highly selective and specific to humidity with a fast response and recovery time. The durability of the sensor was tested by monitoring its response for prolonged hours of operation at extreme conditions of 95% RH. The mechanism of sensing was deduced by impedance, CV, and I-V analysis where the sensor was shown to exhibit a dominating resistive behavior over the entire humidity range with the addition of a slight capacitive nature at higher RH% (>50%). The exceptionally high sensitivity of the F-TEDA-based humidity sensor was obtained because of the synergistic effect of the intrinsic structure of the F-TEDA molecule and the conventional Grotthuss mechanism. Finally, the performance of

the humidity sensor was successfully tested for monitoring human breath rate and touch-less skin moisture sensor. In conclusion, a humidity sensor is realized that can be potentially applied for non-invasive physiological health monitoring as a wearable device.